Nguyen Duc Vu Quyen*, Tran Ngoc Tuyen, Dinh Quang Khieu, Ho Van Minh Hai, Dang Xuan Tin and Kiyoshi Itatani

Oxidation of dibenzothiophene using the heterogeneous catalyst of tungsten-based carbon nanotubes

https://doi.org/10.1515/gps-2017-0189
Received December 24, 2017; accepted April 3, 2018; previously published online May 16, 2018

Abstract: Highly effective tungsten-based carbon nanotubes (W/CNT) were synthesized and used as a heterogeneous catalyst for the oxidation of dibenzothiophene (DBT) with the oxidant H_2O_2. The obtained materials were characterized by modern methods. The Langmuir–Hinshelwood kinetics model described the precursor mechanism of the reaction well through an intermediate compound. The low activation energy showed that the reaction was mainly controlled by diffusion. The positive activation enthalpy proved the endothermic nature of the activation process, and this process did not alter the inside structure of the catalyst. The thermodynamic parameters of the reaction were determined, which implied that the oxidation was endothermic and spontaneous at 303 K. The more negative values of the Gibbs free energy from 283 to 323 K confirmed that the reaction was more favorable at high temperatures. The stability and activity of catalyst were retained after three reaction cycles.

Keywords: kinetics of dibenzothiophene oxidation; Langmuir–Hinshelwood; oxidative desulfurization (ODS); tungsten-based CNTs.

1 Introduction

Petroleum constitutes one of the most important fossil fuels of modern society, which is used to generate electricity, for transportation, and for industrial productions. However, the emission of sulfur compounds in petroleum, which mainly consist of thiols, sulfides, disulfides, and thiophenes, are undesirable during the utilization of petroleum because the combustion of these compounds releases sulfur oxides and oxyacids which are not only toxic to humans and contribute to environmental pollution, such as acid rain, but also cause corrosion to parts of internal combustion engines [1, 2]. Dibenzothiophene (DBT) is one of sulfur compounds that is difficult to remove from diesel by conventional desulfurization processes [3]. Therefore, the removal of sulfur compounds from the fuel has aroused the interest of many scientists.

Hydrodesulfurization (HDS) is a catalytic chemical process that is widely used to remove sulfur. This process, however, was limited for treating DBTs, especially those having alkyl substituents on their 4- and/or 6-position [4]. Thus, the petroleum with a low sulfur level requires critical conditions (high pressure and temperature) and special active catalysts [5]. New methods of reduction of the sulfur content in petroleum are needed to meet future legislations on the sulfur content, e.g. <10 ppm [6]. Oxidative desulfurization (ODS) is considered to be one of the promising methods for deep desulfurization of petroleum. In comparison with HDS, ODS can be carried out at room temperature and under atmospheric pressure. By this method, the sulfur compounds will be oxidized into stable and strongly polar compounds, such as sulfone or sulfoxide, that can be separated from petroleum by extraction into a polar solvent [7–11]. The catalyst used for ODS can be homogeneous such as HCOOH [12] or Na_2WO_4 [13], or heterogeneous such as Cu/TS-1 [14], a heteropolyacid (HPA) catalyst such as $H_3PW_{12}O_{40}$ (HPW) [15], and, especially, tungsten oxide supported on carriers [3, 16–18] that shows high effectiveness. With different carriers, the catalytic ability of tungsten oxide can be different based on the interaction between the catalyst and the carrier. In many studies, silica-based carriers were employed, such as SiO_2, MCM-41, MIL-101, so on, but thiophene removal was not high at room temperature (~70%) [3, 16–18].

Nanocarbon is well known as an excellent adsorbent not only of heavy metals and organic pigments but also

***Corresponding author: Nguyen Duc Vu Quyen,** Department of Chemistry, College of Sciences, Hue University, Hue, Vietnam, e-mail: ndvquyen.hueuni.edu@gmail.com
Tran Ngoc Tuyen, Dinh Quang Khieu, Ho Van Minh Hai and Dang Xuan Tin: Department of Chemistry, College of Sciences, Hue University, Hue, Vietnam
Kiyoshi Itatani: Department of Materials and Life Sciences, Faculty of Science and Technology, Sophia University, Chiyoda-ku, Tokyo 102-8554, Japan

for sulfur in petroleum when this material is made passive by poly(ethylene glycol) (PEG-200), as shown by Fallah et al. [19]. Nevertheless, the maximum sulfur conversion was ~80% even at high temperature. Zhang et al. [20] employed carbon nanotubes (CNTs) as a good catalyst for DBT conversion only at high temperature (150°C) and with a strong oxidant (oxygen with a flow rate of 150 ml min^{-1}). In development of using CNTs to desulfurize petroleum, no mention has been made of any studies of their use as a carrier for the dispersion of tungsten oxide. The important advantages of CNTs are their high surface area and electron-transport ability, which contribute to the creation of many active catalyst sites. Besides, sulfur-containing aromatic compounds such as DBT can be strongly attracted toward the surface of CNTs because of π–π stacking, which is one of the reasons why the catalyst exhibits high activity for the oxidation of DBT.

In this work, a new material, tungsten dispersed on CNTs (W/CNT), exhibiting high catalytic efficiency for DBT removal in petroleum, was synthesized. The kinetic and thermodynamic studies of DBT conversion using W/CNT catalyst were also carried out.

2 Materials and methods

2.1 Materials

The CNTs were synthesized from liquid petroleum gas (LPG) by chemical vapor deposition (CVD) using Fe/Al_2O_3 as the catalyst. The tubes of the material were uniform with size in the range 30–50 nm (Figure 1).

The resulting CNTs were dispersed in 0.1 M H_2SO_4 solution by ultrasonic stirring for 30 min, and then Na_2WO_4 was added to the CNT suspension again under ultrasonication. The W/CNT material was obtained by drying the above mixture at 80°C until its weight remained unchanged and after heating the obtained solid at 500°C for 1 h.

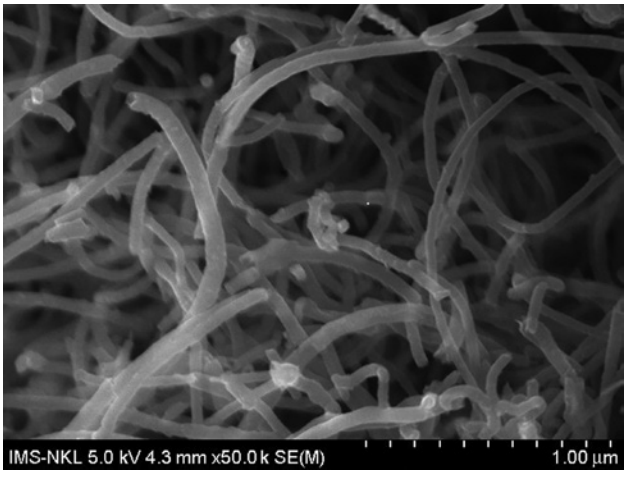

Figure 1: SEM image of CNTs.

2.2 Methods

2.2.1 Characterization of CNTs and W/CNT: The phases of the obtained materials were studied using an X-ray diffractometer (XRD) (model RINT2000/PC; Rigaku, Tokyo, Japan) with $\lambda_{CuK\alpha} = 0.154$ nm. The functional groups on the surface of the materials were identified by a Fourier transform infrared (FT-IR) spectrometer (model IRPrestige-21; Shimadzu, Kyoto, Japan). Energy-dispersive spectroscopy (EDS) was employed to determine the elemental composition of the materials. Raman spectroscopy was used to study the presence of defects on the surface of materials, using a Lab RAM HR800 device (Horiba, Tokyo, Japan). The tube morphology was studied using a field-emission scanning electron microscope (FE-SEM; model S-4800; Hitachi, Tokyo, Japan) and a scanning transmission electron microscope (STEM) attached to the FE-SEM. The specific surface area was measured by nitrogen adsorption/desorption instrument at 77 K (model BELSORP-mini, MicrotrackBEL, Osaka, Japan) and calculated on the basis of Brunauer–Emmett–Teller (BET) theory.

2.2.1 Catalytic studies: Anhydrous DBT (Merck, Germany) was dissolved in *n*-hexane (Daejung Chemicals & Metals Company, Korea) to prepare model oil samples. Catalytic oxidation was carried out in a reactor containing 20 ml of the model oil, 10 ml of acetonitrile, W/CNT, and H_2O_2 solution. The concentration of DBT was determined by UV–vis spectroscopy ($\lambda_{max} = 235$ nm). DBT conversion was calculated using the following expression:

$$H = \frac{(C_0 - C)\cdot 100}{C_0} \quad (1)$$

where H (%) is the DBT conversion, and C_0 and C (mg l^{-1}) are the concentrations of DBT before and after catalysis, respectively.

To determine the effect of the tungsten amount in W/CNT for optimal DBT conversion, samples of W/CNT containing different percentages of tungsten (w/w) were prepared and their DBT conversions were tested. The effect of the ultrasonication time was also studied (0.5–5.0 h).

In catalytic studies, the effect of the molar ratio of O/S (H_2O_2/S) and catalyst dosage for DBT conversion, kinetic, and thermodynamic investigations were carried out. W/CNT was added to the sample at different dosages at 30°C with different molar ratios of O/S. The catalysis was allowed to take place, and the concentration of DBT before and after the catalytic reaction was determined. The kinetic data were inferred from the study of the catalytic ability of W/CNT for different reaction times.

The effect of temperature on the DBT removal reaction was studied from 283 to 323 K. At each temperature, 20 ml of the model oil sample containing 500 mg l^{-1} of sulfur and 10 ml of acetonitrile was stirred with 5 g l^{-1} of W/CNT for different times. Consequently, the Gibbs free energy ($\Delta G°$), enthalpy (ΔH), entropy (ΔS), activation energy (E_a), and activation enthalpy (ΔH^*) of adsorption were determined.

The recycling ability of the catalyst was studied. The catalyst was filtered and washed by *n*-hexane, acetonitrile, and distilled water and then dried at 80°C for 24 h before reuse with the initial sulfur concentration of 491 mg l^{-1}.

3 Results and discussion

3.1 Determination of suitable synthesis conditions of W/CNT

The synthesis of W/CNT was carried out by combining ultrasonic and mechanical stirring of a mixture of 0.1 M H_2SO_4 solution of CNTs and Na_2WO_4. During the synthesis, the catalytic efficiency of W/CNT material invariably depends on the tungsten amount (percentage of tungsten in catalyst) and ultrasonication time. Consequently, two groups of samples were prepared with different amounts of tungsten (0.5–10.0%) and different ultrasonic times (0.5–5.0 h) at the same initial sulfur concentration of 520 mg l^{-1}. The dosage of W/CNT, reaction time, and O/S molar ratio were fixed at 5.0 g l^{-1}, 3.0 h, and 13.7, respectively. The W/CNT material was obtained after ultrasonic-assisted mechanical stirring of the mixture of CNTs, H_2SO_4, and Na_2WO_4 solution, prior to the filtering and drying in a furnace at 773 K. DBT conversions of samples were determined based on initial and remaining concentrations of DBT, as shown in Figure 2.

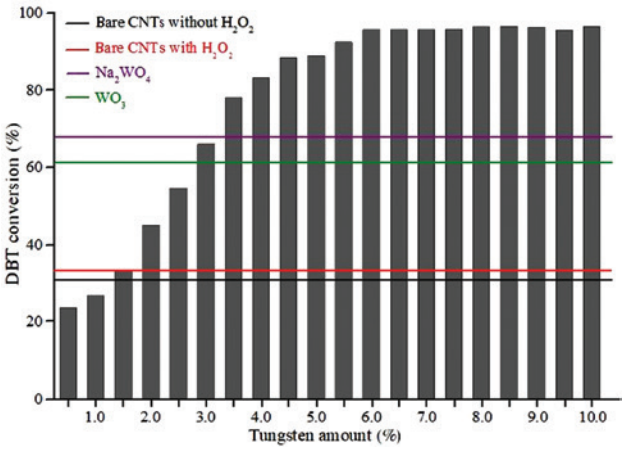

Figure 2: Effect of tungsten amount in W/CNT for DBT conversion.

Figure 2 presents the effect of the amount of tungsten in W/CNT on DBT conversion at room temperature. As can be seen from the figure, bare CNTs with and without H_2O_2 showed the same DBT conversion of ~30%, indicating that the conversion of DBT is due to the adsorption and liquid/liquid extraction (20%) and that the CNTs without tungsten did not catalyze any DBT oxidation reaction. Meanwhile, W/CNT catalyzed the DBT oxidation reaction and its catalytic ability depended on the amount of tungsten. DBT conversion increased significantly from 3.8% to 95.9% as the amount of tungsten was increased from 0.5% to 6.0%, and then remained constant at ~95% as the tungsten content further increased. This means that tungsten acts as the catalytic sites, and the more the amount of tungsten, the more the number of catalytic sites, resulting in enhanced DBT conversion. A high amount of tungsten in W/CNT may make the catalytic sites to saturate, leading to unchanged DBT conversion. Therefore, a tungsten content of 6.0% was taken for the optimal catalytic activity of W/CNT. In comparison with some other tungsten-containing catalysts (shown in Table 1), although the tungsten content used in our catalyst was lower, DBT conversion still was higher or equal at room temperature. As can be seen, CNTs can act as a carrier for the effective enhancement of the number of catalytic sites. Also, the π–π interaction between the carbon rings of CNTs and DBT increases the attraction of DBT toward the surface of the catalyst.

The homogeneous catalyst Na_2WO_4 without carrier yielded lower DBT conversion (67.9%) than the heterogeneous catalyst W/CNT, which was unresponsive for deep desulfurization. This was also proved in some studies such as those of Al-Shahrani et al. [2], who found that the DBT conversion was only 20% at room temperature even though they used a higher dosage of the catalyst (10.8%) at 60°C as in the study of Chao et al. [13]. The same

Table 1: Catalytic oxidation conditions of DBT in some studies.

Catalyst	Tungsten amount (%)	O/S molar ratio	*T* (°C)	DBT conversion (%)	Catalyst dosage (g l^{-1})	References
W/CNTs	6.0	13.7	28	95.9	5.0	Present study
W/MCM-41	15.0	5.0	40	69.6	4.0	[16]
			70	98.0		
W/MIL-101	43.6	50.0	45	91.0	7.5	[21]
W/CeO_2	26.7	5.0	30	91.6	6.0	[22]
W/SiO_2	13.3	4.3	60	75.5	1.5	[23]
	23.5			99.7		
	38.0			100.0		

Initial sulfur concentration = 500 mg l^{-1}; MIL-101 is a metal organic framework material; MCM-41 is a mesoporous silica material.

experiment was carried out with the heterogeneous catalyst WO_3 without CNTs. The low DBT conversion (~60%) proved the important role of CNTs as the catalyst carrier.

The effect of ultrasonication time at 40°C during W/CNT synthesis on DBT conversion was investigated. The result showed that DBT conversion increased with an increase in ultrasonication time and only slightly changed when applied for more than 1 h. It is worth noting that the significant increase of DBT conversion of ~78% was obtained for ~30 min of ultrasonication and the DBT conversion reached 96% only after 1 h of treatment compared to 50% with W/CNT prepared without ultrasonication. This means that ultrasonic-assisted mechanical stirring dispersed tungsten efficiently and homogeneously on the CNTs. Therefore, the suitable ultrasonic time for synthesizing W/CNT was taken as 1 h.

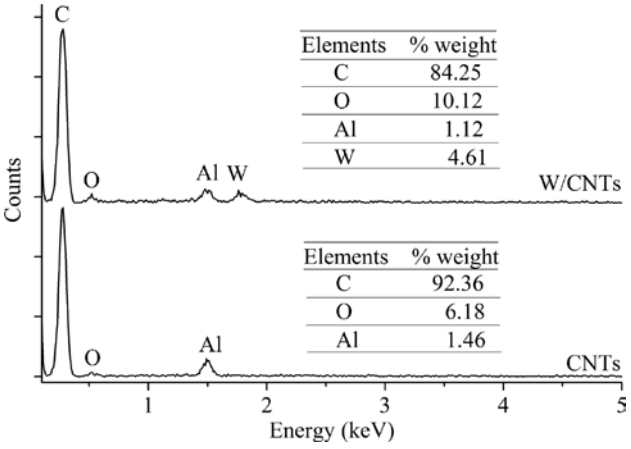

Figure 4: EDX analyses of CNTs and W/CNT.

3.2 Charaterization of W/CNT

The XRD patterns of CNTs and W/CNT are shown in Figure 3. The crystal phase of carbon in both materials, which was confirmed by the diffraction peak at 2θ of ~26° (JCPDS card files, no 41-1487), corresponded with the (002) lattice face [24, 25]. For W/CNT, the appearance of broad diffraction lines at 2θ from 26° to 30 corresponding to the (002) and (020) lattice faces, as well as two peaks at ~35 corresponding to the (022) and (202) lattice faces, proved the presence of tungsten on the surface of CNTs [26].

EDS analysis of CNTs and W/CNT (Figure 4) provided evidence for the presence of graphite as the main component of the samples (92.36% for CNTs and 84.25% for W/CNT). The weight percent of tungsten in the material inferred from EDS analysis of W/CNT was 4.61%. The weight percent of oxygen in the W/CNT sample was higher than that in the CNT samples, which could be explained by the dispersion of oxygen from WO_3 on the surface of the material.

Some organic functional groups of CNTs and W/CNT were detected from the FT-IR spectra (Figure 5). For both of materials, the broad absorption band at ~3447 cm^{-1} was due to the stretching vibration of the C–OH groups on the surface of the materials. The peaks from 1562 to 1700 cm^{-1} for W/CNT and the broad band at ~1629 cm^{-1} for CNTs were attributed to the H–O–H bending vibration of the adsorbed H_2O molecules, the C=C groups in C-sp^2 of graphite, and C=O groups relating to the oxygen-containing groups such as –COOH. For W/CNT, the peak band at ~855.4 cm^{-1} was ascribed to the vibration of the W–O–W bond, which was not found in the case of the bare CNTs [27, 28].

Figure 6 shows a selected region of the Raman spectra of the CNTs and W/CNT. Both CNTs and W/CNT show two peaks at ~1320 cm^{-1} called the D band (D for disorder) and

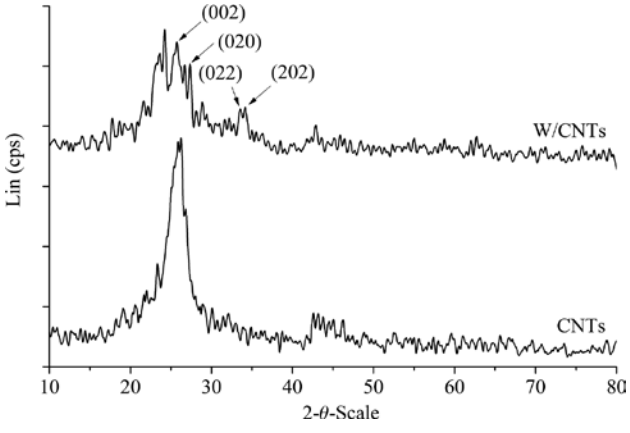

Figure 3: XRD patterns of CNTs and W/CNT.

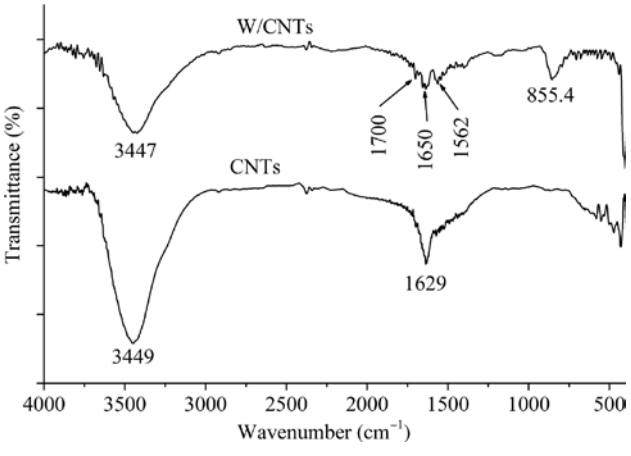

Figure 5: FT-IR spectra of CNTs and W/CNT.

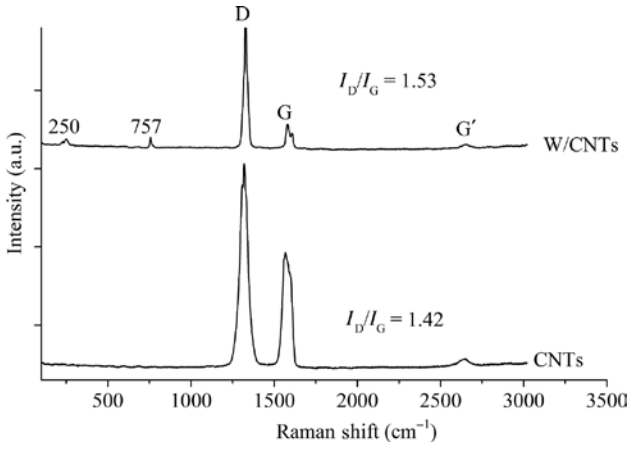

Figure 6: Raman spectra of CNTs and W/CNT.

1566 cm^{-1} called the G band (G for graphite). The graphitic tubes were characterized by the G band. Meanwhile, the D band confirmed the presence of defects within the hexagonal graphitic structure. The G′ band at 2642 cm^{-1} was an overtone of the D band. The density of defects in the CNT structure could be estimated by the ratio of the integrated intensities of the D and G bands (I_D/I_G) [27–29]. Thus, a higher value of I_D/I_G of W/CNT (1.53) is indicative of higher defects and disorders of the graphitized structures in comparison with CNTs (1.42) due to the bonding between WO_3 and C-sp^2 of the graphitic tubes. Compared to those of CNTs, the Raman vibrations of W/CNT centered at 250 and 757 cm^{-1} were attributed to the W–O bonds [27, 28]. The presence of these peaks in the Raman spectrum of W/CNT confirmed that WO_3 was dispersed on the surface of CNTs.

Figure 7 shows the FE-SEM and STEM images of the W/CNT. These STEM images show that the long tubular structure with tube diameter of ~30–50 nm was still maintained after dispersing tungsten. WO_3 particles could not be observed on the SEM and STEM images because of their small size. The surface area based on the BET model was 139 m^2 g^{-1}.

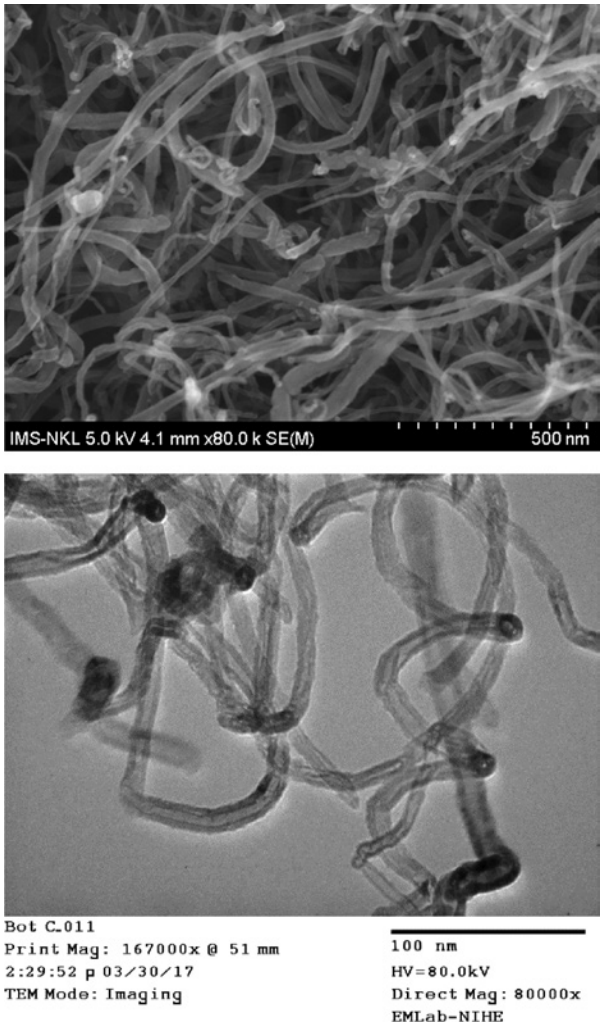

Figure 7: FE-SEM and STEM images of W/CNT.

3.3 DBT catalytic oxidation

3.3.1 Effect of molar ratio of O/S

The effect of the molar ratio O/S on the DBT oxidation conversion was investigated from 1.7 to 51.2. With initial sulfur concentration of 529 mg l^{-1}, the catalyst dosage of 5.0 g·l^{-1}, and at room temperature, DBT oxidation conversion increased remarkably up to 96% as the O/S molar ratio was increased from 1.7 to 17.0, but varied only unremarkably afterward.

Therefore, the O/S molar ratio of 17.0 was chosen for further experiments. This ratio is higher than that reported by some other authors, as shown in Table 1. However, it is worth noting that the present study was conducted under ambient conditions with low tungsten content.

3.3.2 Effect of W/CNT dosage

An increase in trend of DBT conversion was observed (from 77% to 94%) when the dosage of W/CNT was increased from 1.25 to 5 g l^{-1}. Subsequently, DBT conversion reached 98% when the W/CNT dosage was 6.25 g l^{-1} and more, with the initial sulfur concentration of 525 mg l^{-1}, O/S molar ratio of 17.0, and at room temperature (28°C). Therefore, the suitable W/CNT dosage was chosen as 5 g l^{-1} for deep desulfurization.

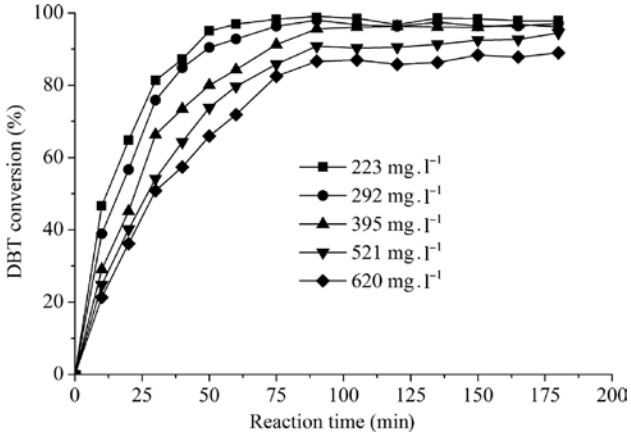

Figure 8: Effect of reaction times in DBT conversion of W/CNT at different initial DBT concentrations.

3.3.3 Catalytic kinetics

Figure 8 presents the reaction kinetics of DBT oxidation with different initial concentrations of DBT. As seen from Figure 8, the DBT conversion increased with increase in contact time. Because of the increase of the initial sulfur concentration without the increase in dosage of the catalyst (5 g l^{-1}) and oxidant amount (O/S molar ratio of 17.0), the efficiency of the reaction decreased from ~95% to 86% corresponding the initial sulfur concentration from 223 to 620 mg l^{-1}, and the equilibrium reaction time increased from 60 to 90 min.

The Langmuir–Hinshelwood (LH) kinetic model is popularly used to explain the mechanism of heterogeneous catalytic reactions [30, 31]. In this model, the reactants are adsorbed on the catalytic centers (S) to form the intermediates (A…S or B…S), and then these intermediates react together to form the products. The reaction can be describes as follows:

$$A + S \rightleftarrows A\ldots S \quad (2)$$

$$B + S \rightleftarrows B\ldots S \quad (3)$$

$$AS + BS \rightarrow \text{products} \quad (4)$$

It is assumed that Equation (4) is the rate-limiting step. The LH expression is given by Equation (5):

$$r = -\frac{dC}{dt} = \frac{k_r KC}{1 + KC} \quad (5)$$

where r represents the rate of oxidation (mg l^{-1} min^{-1}), k_r is the LH rate constant (mg l^{-1} min^{-1}), C is the DBT concentration (mg l^{-1}), and K is the equilibrium adsorption constant (l mg^{-1}).

During the catalytic process, an intermediate is formed, which hinders the determination of the reaction kinetics because of the competition between adsorption and catalysis. Therefore, in very early time, the effect of the intermediate is supposed to be unremarkable. Then, the initial rate of reaction, r^0, as a function of the initial concentration of sulfur, C^0, is calculated by Equation (6):

$$r^0 = \frac{k_r KC^0}{1 + KC^0} \quad (6)$$

which can be linearizied as in Equation (7):

$$\frac{1}{r^0} = \frac{1}{k_r} + \frac{1}{k_r KC^0} \quad (7)$$

$KC << 1$ means that means the DBT is weakly adsorbed on the catalyst, and Equation (5) can be rewritten as Equation (8) and linearized as the first-order kinetic equation (Eq. 9):

$$r = k_r KC \quad (8)$$

$$\ln\frac{C^0}{C} = k_1 t \quad (9)$$

where k_r is replaced by the first-order rate constant, k_1 (min^{-1}).

Figure 9 shows the linear plots of $\ln(C^0/C)$ versus the reaction time (t). As seen from Figure 9, the high determination coefficients (0.987–0.999) for all initial concentrations indicate that the kinetic data fit well the first-order kinetics model. The value of k_1 was obtained from the slope of the linear regression line shown in Table 2.

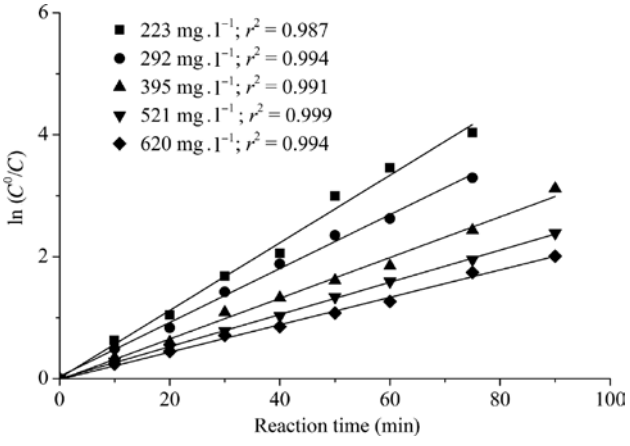

Figure 9: First-order kinetic study of the catalytic oxidation of DBT at different initial DBT concentrations.

Table 2: First-order kinetic parameters of the catalytic oxidation of DBT at different initial DBT concentrations.

C^0 (mg l^{-1})	k_1 (min^{-1})	r^0 (mg l^{-1} min^{-1})
223	0.05540	12.35
292	0.04417	12.89
395	0.03350	13.18
521	0.02635	13.73
620	0.02230	13.83

As can be seen from Table 2, the higher initial DBT concentration, the higher the initial rate and the lower rate constant. The initial concentration provides an important driving force to overcome all the mass transfer resistance of DBT between the aqueous solution and the W/CNT surface. As a result, a high initial DBT concentration will enhance the initial rate. The mass of the catalyst and oxidant reagent is fixed, so the rate constant is reduced as a result of the decrease in O/S molar ratio and the number of DBT/catalytic sites.

The plot $1/r^0$ versus $1/C^0$ following LH kinetic model is shown in Figure 10. The correlation coefficient for the LH kinetic equation was nearly unity ($r^2 = 0.991$), indicating that the DBT catalytic oxidation data fitted well with LH kinetic model. The LH reaction rate (k_r) and equilibrium constant (K) of the adsorption of DBT onto W/CNT were obtained from the slope and the intercept of regression line, which were 14.84 (mg l^{-1} · min^{-1}) and 0.022 (l mg^{-1}), respectively.

The values of the rate constants at different temperatures were obtained from the first-order kinetic equation, as shown in Figure 11 and Table 3.

Table 3 shows that the reaction rate constant (k_1) or the reaction rate (r) or DBT conversion increases with temperature. In other words, the reaction is more favorable at high temperature.

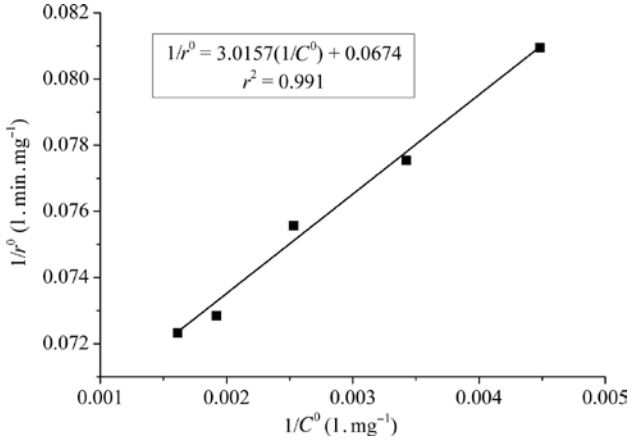

Figure 10: Langmuir–Hinshelwood kinetic model of the catalytic oxidation of DBT.

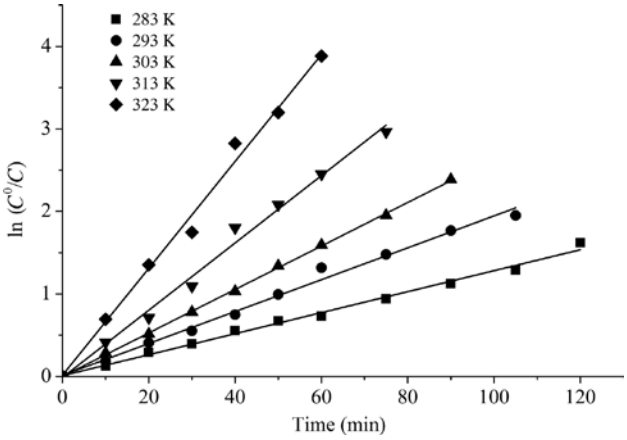

Figure 11: First-order kinetic studies of the catalytic oxidation of DBT at different temperatures.

Table 3: First-order kinetic parameters of the catalytic oxidation of DBT at different temperatures.

Temperature (K)	Correlation coefficient (r^2)	k_1 (min^{-1})
283	0.992	0.01272
293	0.991	0.01932
303	0.999	0.02635
313	0.989	0.04079
323	0.989	0.06476

The activation energy (E_a) was determined by the Arrhenius equation (Eq. 10)

$$k_T = A \cdot e^{-E_a/RT} \tag{10}$$

Taking the natural logarithm of both sides of Equation (11), one obtains

$$\ln k_T = \ln A - \frac{E_a}{RT} \tag{11}$$

where A is the pre-exponential factor, R is the universal gas constant (8.314 J mol^{-1} K^{-1}), and T is absolute temperature (K).

Figure 12A shows the linear plot of ($\ln k_T$) versus $1/T$. The value of E_a could be obtained from the slope ($-E_a/R$). The obtained E_a value calculated by the Arrhenius equation was 30.38 kJ mol^{-1}. The low activation energy (below 42 kJ mol^{-1}) implies that the movement of the reactants to an external surface of catalyst is controlled by diffusion.

The thermodynamic parameters of activation were evaluated to estimate whether there is any complex formation prior to the final adsorption. They are obtained by

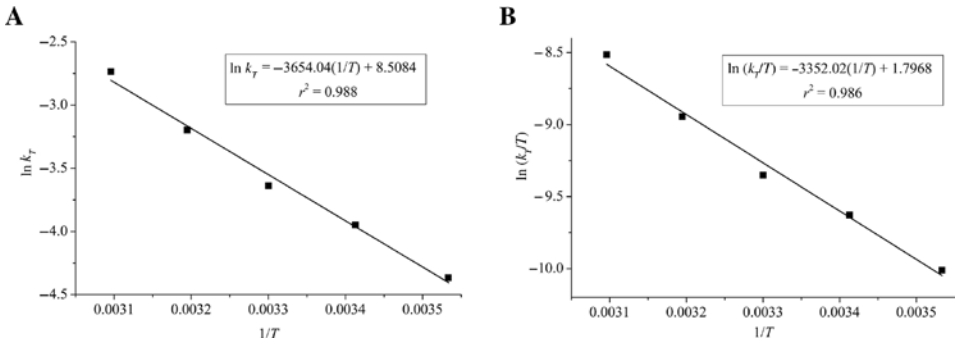

Figure 12: (A) Arrhenius and (B) Eyring equations for DBT catalytic oxidation.

applying the Eyring equation in the linear form, which is expressed as follows:

$$\ln\frac{k_T}{T} = -\frac{\Delta H^{\#}}{RT} + \ln\frac{k_B}{h} + \frac{\Delta S^{\#}}{R} \tag{12}$$

where k_T is the rate constant equal to the rate constant in the first-order model, k_B (1.3807×10^{-23} J K^{-1}) is the Boltzmann constant, and h (6.621 J s) is the Planck constant.

From the linear plot of $\ln(k/T)$ versus $1/T$, the valued s of $\Delta S^{\#}$ and $\Delta H^{\#}$ were calculated from the slope ($-\Delta H^{\#}/T$) and the y-intercept $[\ln(k_B/h)+(\Delta S^{\#}/R)]$. The linear plot of $\ln(k/T)$ versus $1/T$ is shown in Figure 12B. The activation parameters for DBT catalytic oxidation are shown in Table 4.

The positive value of $\Delta S^{\#}$ (468.28 J mol^{-1} K^{-1}) suggests the possibility of formation of an activated complex (metal peroxide intermediate) between DBT and H_2O_2 on the catalyst. Also, the positive value of $\Delta S^{\#}$ normally reflects significant changes occurring in the internal structure of the catalyst during the catalytic process. The value of $\Delta H^{\#}$ (27.87 kJ mol^{-1}) suggests that the formation of the activated complex was endothermic. The large negative values of $\Delta G^{\#}$ imply that the formation of the activated complex occurred spontaneously and favorably at high temperature.

The Gibbs free energy (ΔG°) of reaction was determined by Equation (13), while the enthalpy (ΔH°) and entropy (ΔS°) parameters were calculated using the Van't Hoff equation (Eq. 14 and Figure 13).

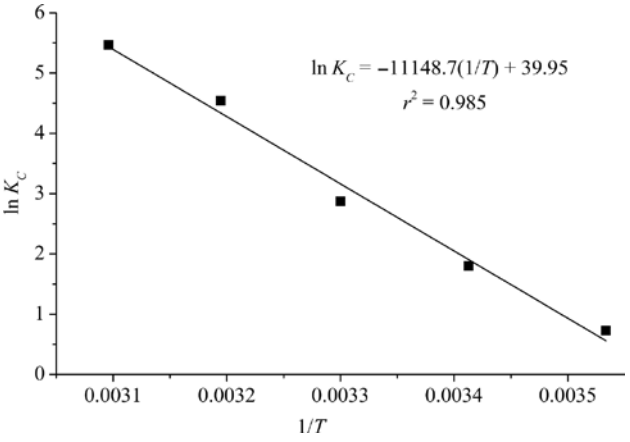

Figure 13: Van't Hoff plot for DBT catalytic oxidation.

$$\Delta G^{\circ} = -RT\ \ln K_C \tag{13}$$

$$\ln K_C = -\frac{\Delta G^{\circ}}{RT} = \frac{\Delta S^{\circ}}{R} - \frac{\Delta H^{\circ}}{RT} \tag{14}$$

The thermodynamic nature of the reaction was examined through the thermodynamic parameters ΔG°, ΔH°, and ΔS° calculated from Equations (13) and (14), and are shown in Table 5.

The positive value of standard enthalpy change ($\Delta H^{\circ} = 92.69$ kJ mol^{-1}) confirmed the endothermic nature of catalytic oxidation. The positive value of standard entropy (ΔS° 322.18 J mol^{-1} K^{-1}) demonstrates that the reaction enhances the randomness at the liquid–solid interface of

Table 4: Activation parameters for DBT catalytic oxidation.

Temperature (K)	$\Delta H^{\#}$ (kJ mol^{-1})	$\Delta S^{\#}$ (J mol^{-1} K^{-1})	$\Delta G^{\#}$ (kJ mol^{-1})
283	27.87	468.28	−104.65
293			−109.34
303			−114.02
313			−118.70
323			−123.39

Table 5: Thermodynamic parameters of DBT catalytic oxidation.

Temperature (K)	ΔH° (kJ mol^{-1})	ΔS° (J mol^{-1} K^{-1})	ΔG° (kJ mol^{-1})
283	92.69	332.18	−1.31
293			−4.64
303			−7.96
313			−11.28
323			−146.01

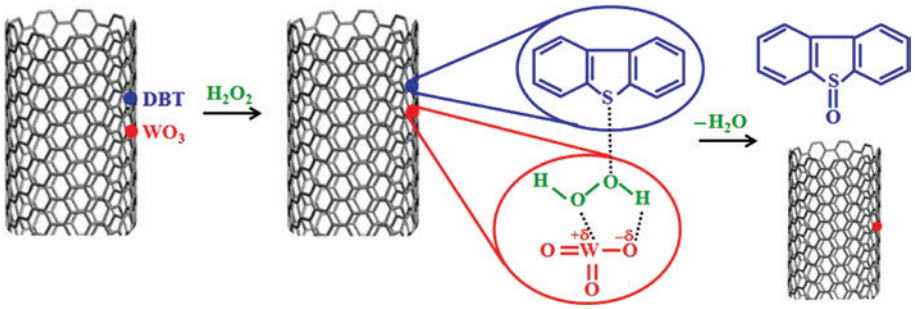

Scheme 1: Proposed mechanism of the catalytic oxidation of DBT to DBTS.

the system as a result of the increase in the number and kinds of molecules in the mixture after the reaction. The Gibbs free energy ($\Delta G°$) at different temperatures had negative values, indicating that DBT oxidation was spontaneous and favorable at high temperature.

The final product, dibenzothiophene sulfone (DBTS), was analyzed by gas chromatography-mass spectrometry (GC-MS; not shown here). In *n*-hexane solvent, the retention times of DBT and DBTS were 16.7 and 18.7 min, respectively. After the oxidation, the oxidation number of sulfur atoms in DBT increased to +2 in sulfoxide and +4 in sulfone. Based on the kinetic and thermodynamic studies, the proposed mechanism of DBT oxidation over W/CNT can be described as in Scheme 1 [32, 33].

The W/CNT with high surface area and active tungsten sites adsorbed the reactants on its surface. This adsorption should be related to the coordination of tungsten toward the free electron pairs of sulfur and the formation of hydroperoxide tungstate through the nucleophilic attack of hydrogen peroxide to tungsten. The π–π stacking hydrophobic interaction between the sp^2-carbon of graphite and aromatic rings of DBT was also responsible for the accumulation of the reactant on W/CNT surfaces. The intermediates, including hydroperoxide tungstate and DBT intermediates, react together to provide DBTS.

3.4 Recyclability of catalyst

The possibility to reuse the W/CNT catalyst was evaluated by the determination of DBT conversion and remaining tungsten amount of the catalyst after four reaction cycles. The result showed that the DBT conversion was retained at ~94% after two first cycles and slightly decreased to 80% after the third reaction cycle. This meant that the activity of catalyst was maintained well after three reaction cycles. However, after the fourth cycle, the DBT conversion was strongly reduced to ~25%, which was equivalent to that with bare CNTs (Figure 2). The stability of the catalyst

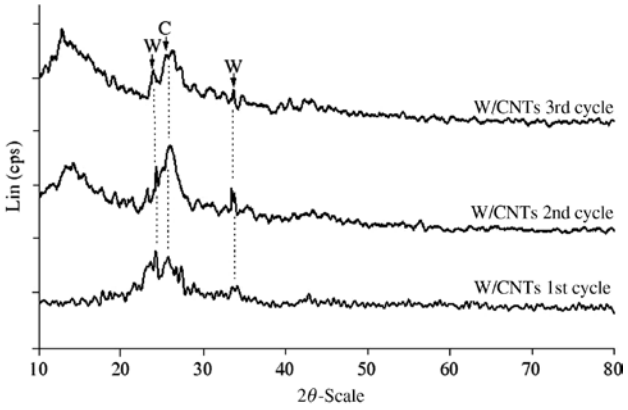

Figure 14: XRD patterns of reused W/CNT.

Table 6: Element compositions of reused catalyst of W/CNT.

Run	wt%			
	W	C	O	Al
1	4.23	83.19	11.21	1.38
2	4.12	84.12	9.54	2.23
3	3.87	85.21	8.79	2.13
4	3.25	88.23	6.78	1.74

was confirmed by EDS/SEM and XRD analyses, as shown in Figure 14 and Table 6. No remarkable reduction of the amount of tungsten in catalyst was observed, and the WO_3 crystal phase still appeared in the XRD pattern of the catalyst during the three reaction cycles. The activity reduction of the used catalyst could result from the poisoning of the active sites on the catalyst by organic compounds.

4 Conclusions

W/CNT was found to be an efficient catalyst for the oxidation of DBT to DBTS. More than 95% of DBT was oxidized at ambient temperature with the catalyst W/CNT

containing 6.0% tungsten (w/w) and O/S molar ratio 17.0. The DBT conversion reached 95% after 90 min at an initial sulfur concentration of less than 600 mg l^{-1}. The oxidation mechanism of DBT on the W/CNT catalyst followed the LH model. The negative Gibbs free energy variation ($\Delta G°$) and positive enthalpy ($\Delta H°$) in the range of temperature 283–323 K showed that the reaction was spontaneous and an endothermic process.

References

[1] Yang RT, Hernández-Maldonado AJ, Yang FH. *Science* 2003, 301, 79–81.
[2] Al-Shahrani F, Xiao T, Llewellyn SA, Barri S, Jiang Z, Shi H, Martinie G, Green MLH. *Appl. Catal. B* 2007, 73, 311–316.
[3] Ribeiro S, Barbosa ADS, Gomes AC, Pillinger M, Goncalves IS, Cunha-Silva L, Balula SS. *Fuel Process. Technol.* 2013, 116, 350–357.
[4] Houalla M, Broderick DH, Sapre AV, Nag NK, De Beer VHJ, Gates BC, Kwart H. *J. Catal.* 1980, 61, 523–527.
[5] Shiraishi Y, Naito T, Hirai T, Komasawa I. *Chem. Commun.* 2001, 14, 1256–1257.
[6] Kabe T, Ishihara A, Qian W. *Hydrodesulfurization and Hydrodenitrogenation*, Kodansha Scientific, Wiley/VCH: Tokyo, New York, 1999.
[7] Yazu K, Makino M, Ukegawa K. *Chem. Lett.* 2004, 33, 1306–1307.
[8] Campos-Martin JM, Capel-Sanchez MC, Fierro JLG. *Green Chem.* 2004, 6, 557–562.
[9] Garcia-Gutierrez JL, Fuentes GA, Hernandez-Teran ME, Murrieta F, Navarrete J, Jimenez-Cruz F. *Appl. Catal. A: Gen.* 2006, 305, 15–20.
[10] Wang D, Qian EW, Amano H, Okata K, Ishihara A, Kabe T. *Appl. Catal. A: Gen.* 2003, 253, 91–99.
[11] Tam PS, Kittrell JR, Eldridge JW. *Ind. Eng. Chem. Res.* 1990, 29, 321–324.
[12] Yao X, Wang S, Ling F, Li F, Zhang J, Ma B. *J. Fuel Chem. Technol.* 2004, 32, 318–322.
[13] Chao Y, Li H, Zhu W, Zhu G, Yan Y. *Pet. Sci. Technol.* 2010, 28, 1242–1249.
[14] Jose N, Sengupta S, Basu JK. *Fuel* 2011, 90, 626–632.
[15] Tang L, Luo G, Zhu M, Kang L, Dai B. *J. Ind. Eng. Chem.* 2013, 19, 620–626.
[16] Abdalla ZEA, Li B, Han C, Mustafa B. *Jordan J. Chem.* 2010, 5, 33–45.
[17] Kong L, Li G, Wang X. *Catal. Lett.* 2004, 92, 163–167.
[18] Zhang M, Zhu W, Li H, Xun S, Ding W, Liu J, Zhao Z, Wang Q. *Chem. Eng. J.* 2013, 243, 386–393.
[19] Fallah RN, Azizian S, Dwivedi AD, Sillanpaa M. *Fuel Process. Technol.* 2015, 130, 214–223.
[20] Zhang W, Zhang H, Xiao J, Zhao Z, Yu M, Li Z. *Green Chem.* 2014, 16, 211–220.
[21] Hu X, Lu Y, Dai F, Liu C, Liu Y. *Microporous Mesoporous Mater.* 2012, 170, 36–44.
[22] Li Y, Zhang M, Zhu W, Li M, Xiong J, Zhang Q, Weia Y, Li H. *RSC Adv.* 2016, 6, 68922–68928.
[23] Zhu W, Gu Q, Hu J, Wu P, Yin S, Zhu F, Zhang M, Xiong J, Li H. *J. Porous Mater.* 2015, 22, 1227–1233.
[24] Cao A, Xu C, Liand J, Wu D, Wei B. *Chem. Phys. Lett.* 2001, 344, 13–17.
[25] Zhang J, Li J, Cao J, Qian Y. *Mater. Lett.* 2008, 62, 1839–1842.
[26] Martínez-de la Cruz A, Sánchez Martínez D, López Cuéllar E. *Solid State Sci.* 2010, 12, 88–94.
[27] Zhou MJ, Zhang N, Hou ZH. *Int. J. Photoenergy* 2014, 2014, 1–6.
[28] Guo J, Li Y, Zhu S, Chen Z, Liu Q, Zhang D, Moon W, Song D. *RSC Adv.* 2012, 2, 1356–1363.
[29] Sui XM, Giordani S, Prato M, Wagner HD. *Appl. Phys. Lett.* 2009, 95, 233113.
[30] Khezrianjoo S, Revanasiddappa HD. *Chem. Sci. J.* 2012, 2012, 1–7.
[31] Kumar KV, Porkodi K, Rocha F. *Catal. Commun.* 2008, 9, 82–84.
[32] Long Z, Yang C, Zeng G, Peng L, Dai C, He H. *Fuel* 2014, 130, 19–24.
[33] Zhang M, Zhu W, Li H, Xun S, Li M, Li Y, Wei Y, Li H. *Chin. J. Catal.* 2016, 37, 971–978.